Physics – Uspekhi **58** (11) 1095 – 1105 (2015)

INSTRUMENTS AND METHODS OF INVESTIGATION PACS numbers: **07.60. – j**, **42.30. – d**, **42.79. – e**

Aperiodic multilayer structures in soft X-ray optics

A S Pirozhkov, E N Ragozin

DOI: 10.3367/UFNe.0185.201511d.1203

Contents

1. Introduction **1095**
2. Multilayer mirrors based on aperiodic structures **1096**
2.1 History of the problem and the first aperiodic X-ray multilayer mirrors; 2.2 Optimization criteria and calculation of aperiodic multilayer mirrors. Inclusion of transition layers
3. Aperiodic normal-incidence Mo/Si multilayer mirrors and their application in experiments **1099**
4. Broadband normal-incidence multilayer mirrors in the wavelength range $\lambda \leqslant 12.5$ nm **1102**
5. Broadband polarization elements based on aperiodic structures **1102**
6. Aperiodic multilayer mirrors as elements of attosecond soft X-ray optics **1103**
7. Conclusions **1104**
References **1104**

Abstract. We review a series of studies that address the development and application of aperiodic multilayer structures (aperiodic multilayer mirrors) as soft X-ray (SXR) ($\lambda \approx 4-40$ nm) optical elements. We discuss the potential of such structures for reflecting SXR radiation in a broad wavelength range, primarily at normal radiation incidence, and as polarization elements (broadband polarizer mirrors and phase shifters). The results of multiparametric optimization are presented, and experimental data for aperiodic Mo/Si ($\lambda \geqslant 12.5$ nm) multilayer mirrors are outlined. The feasibility of advancing to the $\lambda \leqslant 12.5$ nm domain by using other materials is examined, and the capabilities of aperiodic structures as elements of attosecond SXR optics are discussed.

Keywords: soft X-ray/EUV optics, aperiodic multilayer structures, broadband multilayer mirrors, polarization optics, attosecond optical elements, imaging spectrometers

1. Introduction

More than 40 years have passed since the advancement and realization of the idea of an X-ray multilayer mirror and a consistent theoretical analysis of this problem [1–4]. This period has seen the development of methods for synthesizing, characterizing, and calculating multilayer optics in a broad wavelength range in the vacuum ultraviolet (VUV) and X-ray spectral regions (≈ 50 nm – 0.2 Å), which approximately corresponds to a photon energy range of 25 eV–70 keV. The literature on these subjects is quite voluminous; in particular, one of the reviews published recently in *Phys. Usp.* discussed the problems of fabrication, metrology, and application of high-precision imaging multilayer optics [5]. The interest was focused primarily on periodic multilayer structures capable of providing — for a fixed angle of radiation incidence — a rather high reflection coefficient in a relatively narrow wavelength range. The reflection coefficient $R(\lambda)$ of a periodic structure has the shape of a resonance curve and attains its maximum at the wavelength that satisfies the Bragg–Wolf condition,

$$\lambda_0 \approx \frac{2d\langle n\rangle \cos\theta}{m}\,, \tag{1}$$

where d is the structure period (i.e., the sum of the thicknesses of layers A and B alternating in the structure [1]), $\langle n\rangle$ is the period-averaged value of the index of refraction, θ is the angle of incidence, and m is the interference order. The relative width $\Delta\lambda_{1/2}/\lambda_0$ of the resonance depends on several factors — the absorption coefficients of the materials in a given spectral range, the number of layers in the multilayer structure, the ratio of the thicknesses of material layers A and B, transition layers — and may range from ~ 0.1 to less than 0.01.

Multilayer mirrors (MMs) based on periodic structures, or periodic MMs, almost exactly satisfy the criterion of the maximum reflection coefficient at a given wavelength and a

A S Pirozhkov Kansai Photon Science Institute,
Japan Atomic Energy Agency,
8-1-7 Umemidai, Kizugawa, Kyoto, 619-0215, Japan
E N Ragozin Lebedev Physical Institute, Russian Academy of Sciences,
Leninskii prosp. 53, 119991 Moscow, Russian Federation
Tel. +7 (499) 132 63 29
E-mail: enragozin@gmail.com
Moscow Institute of Physics and Technology (State University),
Institutskii per. 9, 141700 Dolgoprudnyi, Moscow region,
Russian Federation

Received 25 August 2015
Uspekhi Fizicheskikh Nauk **185** (11) 1203 – 1214 (2015)
DOI: 10.3367/UFNr.0185.201511d.1203
Translated by E N Ragozin; edited by A M Semikhatov

[1] We are dealing with a binary structure $\{A/B\}_N$; under consideration in some special cases are more complex structures (for instance, ternary). We do not take into account here the transition layers with a mixed elemental composition, which inevitably emerge at the interfaces, nor are we dealing with barrier layers, which are intentionally deposited in some cases to prevent the formation of transition layers of substantial thickness (however, see Sections 2.2, 3, and 4).

fixed angle of radiation incidence. Multilayer mirrors have found wide application in the spectroscopy of laboratory plasmas, X-ray astronomy, analytical instrumentation, and the optics of laboratory vacuum ultraviolet and X-ray radiation sources, including synchrotrons and free-electron lasers.

A new area of application of multilayer optics emerged in connection with the development of unique laboratory sources of coherent VUV radiation: high-order harmonics of high-power femtosecond lasers [6, 7] and the frequency comb of high-order harmonics of the radiation of a continuous femtosecond laser, which radiates a frequency comb in the near-infrared (IR) ('optical') region [8, 9].

Apart from periodic multilayer structures (MSs), of interest are aperiodic structures, which are capable of satisfying criteria other than the attainment of the highest possible reflection coefficient at a given wavelength.[2] In the class of aperiodic MSs, it is possible to solve several optimization problems of practical significance to X-ray optics and spectroscopy, including those of the soft X-ray (SXR) [3] range [11]. Among these are, for instance, calculation and fabrication of MSs that provide (i) the maximum uniform reflectivity in a preassigned interval of wavelengths or angles of incidence, (ii) a high polarizing capacity (polarizance) over a broad wavelength range for a fixed angle of radiation incidence, (iii) the maximum reflection coefficient at one or several wavelengths, and (iv) the maximum integral reflection coefficient of one mirror with the inclusion of the spectrum of a radiation source or the maximum integral 'transmission coefficient' of a system comprising a source and a sequence of several MMs and filters.

Aperiodic MSs are promising components of attosecond optics. Specifically, the inclusion of the phase of the amplitude reflection coefficient (along with its modulus) permits finding the aperiodic structures suitable for the reflection of attosecond SXR pulses and controlling their shape and duration [12, 13].

2. Multilayer mirrors based on aperiodic structures

2.1 History of the problem and the first aperiodic X-ray multilayer mirrors

The idea to design a broadband MM with the maximum integral reflection coefficient by treating the thicknesses of individual structure layers as independent variables (optimization parameters) in the solution of a multiparametric optimization problem (the inverse problem of multilayer optics) was presumably first conceived in solving the problems of X-ray astronomy. Meekins et al. [14] set themselves the task of calculating the aperiodic structures having the maximum integral reflection coefficient

$$\Im_\lambda = \int_{\lambda_1}^{\lambda_2} R(\lambda)\,\mathrm{d}\lambda \qquad (2)$$

in the wavelength ranges 30–60 nm (an Ir/Si structure) and 10–30 nm (a Pt/Si structure) at near-normal radiation incidence. More recently, attempts were made to calculate and synthesize Mo/Si structures having either the maximum integral or maximum uniform reflection coefficient in a given wavelength interval [15]. In particular, a structure was found that provided a uniform reflectivity $R \sim 30\%$ at normal incidence in the wavelength range 15–17 nm. Also considered was the problem of an MM capable of reflecting SXR radiation at two wavelengths [16].

Our main concern in this paper is related to the SXR range of the spectrum. Nevertheless, there is no escape from mentioning, even if briefly, the work related to the hard X-ray range. Even in 1994, Joensen et al. analyzed the feasibility of employing grazing-incidence multilayer optics in a Kirkpatrick–Baez astrophysical telescope for the hard X-ray region and reported the synthesis of a W/Si MM intended for the reflection of X-rays with photon energies up to 69 keV (0.18 Å) at a grazing incidence angle of 3 mrad [17] (Fig. 1). The MM 'period' decreased monotonically with depth according to the analytic law

$$d_i = a(b+i)^{-c}\,, \qquad (3)$$

where d_i is the total thickness of the ith layer pair (numbering from the top), $c \approx 0.26$, $b > -1$, and the coefficient a is proportional to the deviation of the real part of the permittivity of the heavy material from unity (W). It was implied that the shorter-wavelength radiation, which experiences lower absorption and therefore penetrates a greater depth, would be reflected from deeper structure layers with the corresponding 'period' satisfying Eqn (1). This approach has come to be known as the concept of an X-Ray Supermirror. Formula (3), which the authors of Ref. [17] obtained, can be derived by solving a series of direct problems of multilayer optics. Calculated in this case is the reflection coefficient of a given structure, whose parameters are varied, and the result, i.e., the $R(\lambda)$ profile, is compared with the desired profile.

Analytic [18] and numerical [19] methods were proposed for designing aperiodic mirrors with a prescribed spectral, $R(\lambda)$, or angular, $R(\theta)$, reflectivity profile (i.e., methods for the solution of the inverse problem) in the hard X-ray range. Work in this area of research enjoys application for designing

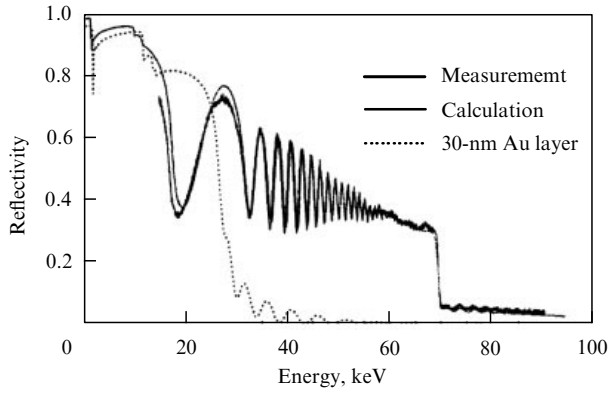

Figure 1. Calculated and measured reflection coefficients of a W/Si 'supermirror' at a grazing incidence angle of 3 mrad. The calculation assumes an interfacial roughness of 4.5 Å. Plotted for comparison is the calculated reflection coefficient of a gold coating 300 Å in thickness [17].

[2] Strictly speaking, the structure that maximizes the reflection coefficient at a preselected wavelength is not exactly periodic; however, its departure from the periodic one is small, and the greater the number of layers that 'work' at this wavelength, the smaller the gain in the peak reflectivity.

[3] In the classification of the subranges of the vacuum domain of the electromagnetic spectrum, we adhere to the monograph by Samson [10], who used the term SXR radiation in reference to the wavelength range 2–300 Å.

mirrors for synchrotron radiation channels and increasing the radiation flux produced by an X-ray tube on a sample [20, 21].

2.2 Optimization criteria and calculation of aperiodic multilayer mirrors. Inclusion of transition layers

In this paper, we are primarily concerned with the wavelength interval 3–30 nm, which pertains to the SXR range of the vacuum spectral domain. As is well known, it has been possible to make rather efficient normal-incidence periodic MMs. 'Ordinary' periodic multilayer structures have a relatively narrow ($\Delta\lambda_{1/2}/\lambda \sim 0.01-0.1$) resonance spectral reflectivity profile, which makes them an efficient tool, first and foremost, for constructing quasimonochromatic spectral images. However, a demand also exists for normal-incidence MMs capable of reflecting radiation in a broad spectral wavelength range without changing the radiation incidence angle. Optical configurations that comprise only normal-incidence mirrors are of special value when compared with grazing-incidence configurations, because the former have significantly smaller aberrations and are therefore suited to the construction of optical images, including dispersed spectral images (of course, when it is possible to make the requisite aperiodic structures with a sufficiently high reflection efficiency). In particular, there is a demand for stigmatic (imaging) optical spectral instruments with a broad operating spectral range (of the order of an octave in wavelength, $\Delta\lambda/\lambda \sim 1/2$). This has become possible due to the use of broadband (aperiodic) normal-incidence MMs in combination with diffraction gratings,[4] for instance, with a transmission grating [22] (Fig. 2a) or a reflective grating whose groove spacing varies monotonically over its aperture according to a prescribed law (a so-called varied line-space (VLS) grating) (Fig. 2b) [23]. These imaging diffraction spectrometers simultaneously have a broad operating spectral range, stigmatism, a relatively large acceptance angle, and a high throughput — a combination of properties that was previously inherent only in spectrometers of the visible, ultraviolet, and partly vacuum ultraviolet ranges ($\lambda \geqslant 50$ nm).

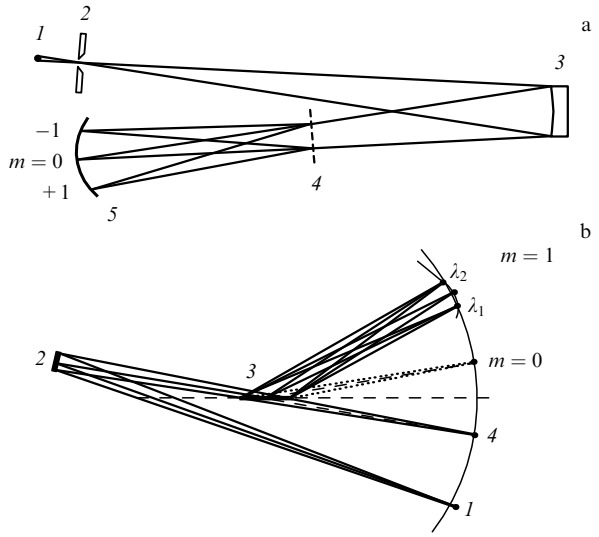

Figure 2. Stigmatic broadband spectrometer comprising an aperiodic multilayer mirror (AMM) with (a) a free-standing transmission diffraction grating or (b) a VLS grating. In Fig. 2a: *1* — source, *2* — entrance slit, *3* — focusing AMM, *4* — free-standing transmission grating, *5* — focal surface, $m = 0, \pm 1$ — diffraction orders. In Fig. 2b: *1* — source, *2* — focusing AMM, *3* — plane VLS grating, *4* — 'vertical' focus of the converging beam, λ_1 and λ_2 — wavelengths for which the coincidence condition for the vertical and horizontal (spectral) foci is strictly fulfilled in paraxial diffracted beams (stigmatism condition).

[4] Dispersed spectral images may also be constructed using multilayer reflective diffraction gratings. The case in point is a concave diffraction grating with a multilayer structure deposited on top of it.

The areas of application of broadband aperiodic mirrors and the instruments made with their use comprise investigations of elementary processes with the participation of multiply charged ions that are conducted using stigmatic spectrographs [22, 24–31]; diagnostics of plasmas, including laser-driven microplasma; recording of the high-order harmonic spectra of laser radiation; control of SXR radiation pulses generated by free-electron lasers [32] or other sources; reflection of attosecond SXR pulses and transformation of their duration [12, 13]; etc. The problem of maximizing the integral 'transmission coefficient' after several successive reflections in a mirror system with the inclusion of the spectrum of the radiation source and filter transmittances arises, in particular, in X-ray lithography. Recently, an Mo/Si MM optimized for maximum uniform reflectivity in the wavelength range 12.5–25 nm at normal radiation incidence was employed in experiments in the conversion of Ti:Sapphire laser radiation ($\lambda \approx 0.8$ μm) to SXR radiation. The frequency up-conversion took place in the reflection from a relativistic plasma wave driven by a multiterawatt laser in a pulsed helium jet (a relativistic 'flying mirror') [33–35].

For the first step, we decided to use a molybdenum–silicon MS, which provides high reflectivity in the domain $\lambda > 12.5$ nm. Later on, we plan to extend our approach to the domain under the L edge of absorption in silicon ($\lambda < 12.5$ nm), which invites the use of other material pairs.

The numerical technique described in this section permits optimizing a multilayer structure for different criteria. The technique under consideration has demonstrated its efficiency in the optimization of aperiodic MSs intended for operation in any subrange of the X-ray spectrum and for different angles (including small grazing angles) of radiation incidence; in this case, the number of structure layers may be quite large ($\sim 10^3$). The main (but not the sole) purpose of our simulations is the quest for aperiodic MSs with as broad a uniform reflection band as possible.

We consider a multilayer structure $\{l_j\}$, $j=1,\ldots,N$, consisting of N alternating levels, which are characterized by complex permittivities of the form $\varepsilon_{A,B} = n_{A,B}^2 = 1 - \delta_{A,B} + i\beta_{A,B}$. For materials consisting of atoms of one sort, the optical constants $\delta_{A,B}$ and $\beta_{A,B}$ are related to the atomic scattering factors $f = f_1 + if_2$ by the formula

$$\begin{pmatrix}\delta\\ \beta\end{pmatrix} = \frac{r_0}{\pi}\,\lambda^2 N\begin{pmatrix}f_1\\ f_2\end{pmatrix} \approx 0.54\times 10^{-5}\,\frac{\rho}{\mu}\,\lambda_A^2\begin{pmatrix}f_1\\ f_2\end{pmatrix},$$

where $r_0 = e^2/m_e c^2 \approx 2.8\times 10^{-13}$ cm is the classical electron radius, N is the atomic number density, and μ is the atomic mass; λ_A is expressed in angstroms and the substance density ρ in grams per cubic centimeter. When a substance consists of atoms of several sorts, a more general expression applies:

$$\begin{pmatrix}\delta\\ \beta\end{pmatrix} \approx 0.54\times 10^{-5}\,\frac{\rho}{\sum_i \alpha_i\mu_i}\,\lambda_A^2\begin{pmatrix}\sum_i \alpha_i f_{1i}\\ \sum_i \alpha_i f_{2i}\end{pmatrix},$$

where α_i is the fraction of atoms of sort i. The data on atomic scattering factors for elements with atomic numbers from 1 to 92 in the 10 eV–30 keV photon energy range are available

from the literature [36, 37]. (Files containing refined atomic scattering factors are available from the site http://henke.lbl.gov/optical_constants/.)

The layer thicknesses l_j are different in general. Unlike the layer thicknesses in a periodic structure, the sums of the thicknesses of neighboring layer pairs are not assumed to be constant with depth in the structure: $l_1 + l_2 \neq l_3 + l_4 \neq \ldots$. The optical path lengths for neighboring layer pairs are also not equal in general: $l_1 n_A + l_2 n_B \neq l_3 n_A + l_4 n_B \neq \ldots$. Furthermore, the existence of a structure period in any sense is not assumed *a priori*.

The structure's reflection coefficient $R_{s,p}(\lambda, \theta)$ for s- and p-polarized radiation incident at an angle θ (the direct problem of multilayer optics) was calculated by the method of recursive relations described in the literature [3, 38] and repeatedly used by several authors. The problem of finding the aperiodic MS that best satisfies some preassigned criterion is referred to as the inverse problem of multilayer optics or the aperiodic MS (AMS) optimization problem. A goal function F_{gf} was specified for $R_{s,p}(\lambda, \theta_0)$ or $R_{s,p}(\lambda_0, \theta)$ (the subscript '0' signifies that the angle of incidence or the wavelength are fixed). The goal function may be specified in some interval of wavelengths or angles of incidence as well as in several isolated intervals. We introduced the norm of the deviation of the reflection coefficient from F_{gf} (the merit function F), which was calculated in the domain of F_{gf} and treated as a function of N variables $\{l_j\}$. A numerical technique was then used to find the AMS by minimizing the functional $F = \int (R(\lambda) - F_{gf})^{2m} \, d\lambda$, $m = 1, 2, \ldots$. In a similar way, the integration could be performed over the photon energy or frequency. The functions F_{gf} and F were selected based on the nature of the problem being solved and predetermined the optimization result. In the optimization of multilayer structures intended for the reflection of ultrashort (atto- and zeptosecond) pulses, the functions also comprised dispersion (phase) characteristics or the properties of reflection pulses (see below). The number of optimization parameters (the dimensionality of space) was equal to the number of layers in the aperiodic structure. To find the extremum of the functional F, in particular, a genetic algorithm and the method of steepest descent were used. To decrease the dependence of the computation time on N, an analytic formula was derived for the partial derivatives of the amplitude reflection coefficient with respect to individual layer thicknesses [11].

We concerned ourselves primarily with multilayer structures and mirrors suitable for operation as the focusing elements of a spectrometer with a broad operating spectral range. Aperiodic MSs of this kind were optimized to achieve the highest uniform reflectivity over a prescribed wavelength range by minimizing the functional

$$F = \int_{\lambda_1}^{\lambda_2} \left(R(\lambda) - R_0\right)^{2m} d\lambda \,.$$

The computationally found aperiodic MSs had a substantially higher integral reflection coefficient than any periodic mirror whose resonance reflection peak was located in the same wavelength interval. Periodic structures served as the initial structures in solving these optimization problems. In this case, it turned out that different initial structures might lead to practically equivalent (from the optimization criterion standpoint) solutions, although their corresponding (optimized) AMSs were substantially different in layer thickness sets $\{l_j\}$. Therefore, the question of finding the absolute (global) minimum of F remained open.

In the calculation of reflection characteristics of MMs, possible imperfections of the fabricated (synthesized) MSs themselves must be taken into account. Among the variety of observed defects (the presence of impurities, departure of layer densities from the tabulated values, the state of the MS surface, etc.), of paramount importance in impairing the optical characteristics of an MS are its interlayer roughness and the formation of transition layers. When individual layers are deposited by sputtering techniques (ion-beam, magnetron, triode sputtering, etc.), the substrate roughness is typically reproduced in the coating, and therefore today the availability of substrates with a roughness smaller than 2 Å permits regarding the roughness problem as being of secondary importance. However, the existence of transition layers, which result from interdiffusion in MS fabrication, has a consequence that the permittivity of pure materials A and B varies from ε_A to ε_B gradually, not abruptly, over the thickness of the transition layer. The degree of mixing and the composition of transition layers depend on the technique and conditions of MS fabrication. In Mo/Si mirrors synthesized by magnetron sputtering at the National Technical University "Kharkov Polytechnic Institute" (KhPI), as suggested by the electron microscopy data for transverse sections of the mirrors, the thickness of an Mo-on-Si transition layer is about 12 Å and the thickness of an Si-on-Mo transition layer is about 6 Å, if the underlying Mo layer is no less than ≈ 20 Å in thickness, this transition layer being close to the silicide $MoSi_2$ in elemental composition [39].

Transition layers in a periodic structure diminish its reflection coefficient. Specifically, in the Mo/Si periodic structure optimized for maximum reflectivity at $\lambda = 13.5$ nm in the ratio of Mo layer thickness and the period, the inclusion of transition layers results in a lowering of the peak reflection coefficient from 74.6% to 71.6%. A more realistic description of the effect of transition layers on the structure reflectivity takes the smooth character of permittivity variation at the interface into account. This inclusion is mathematically achieved, for instance, by a multistep approximation of the transition using a linear interpolation of ε.

Figure 3a shows the reflectivity profile of a periodic MM (Mo/Si, $\lambda_0 = 13.5$ nm) with and without the inclusion of transition layers; shown in Fig. 3b is the behavior of the peak reflectivity when the difference $\varepsilon_{Mo} - \varepsilon_{Si}$ is approximated by a variable number of steps as well as when the transition layer is approximated by a layer with the stoichiometry of the silicide $MoSi_2$. We can see that the peak reflectivity increases slightly and tends to a constant value with an increase in the number of steps. This limit value is approximately 1% higher than the value obtained when the transition layer is included in the form of one layer of the silicide $MoSi_2$. Therefore, it is likely that the approximation of one transition layer of known stoichiometry provides a reasonably good description from the practical standpoint.

In the optimization (in the solution of inverse problems), we introduced a programmable limit on the minimal layer thickness. This stems from the necessity to eliminate physically absurd solutions (the layer thickness cannot be smaller than the size of an atom or a molecule) and improve the stability of the reflection coefficient of the synthesized MS relative to the formation of transition layers (ideally, the thicknesses of 'pure' substance layers should greatly exceed the thicknesses of transition layers). We determined an

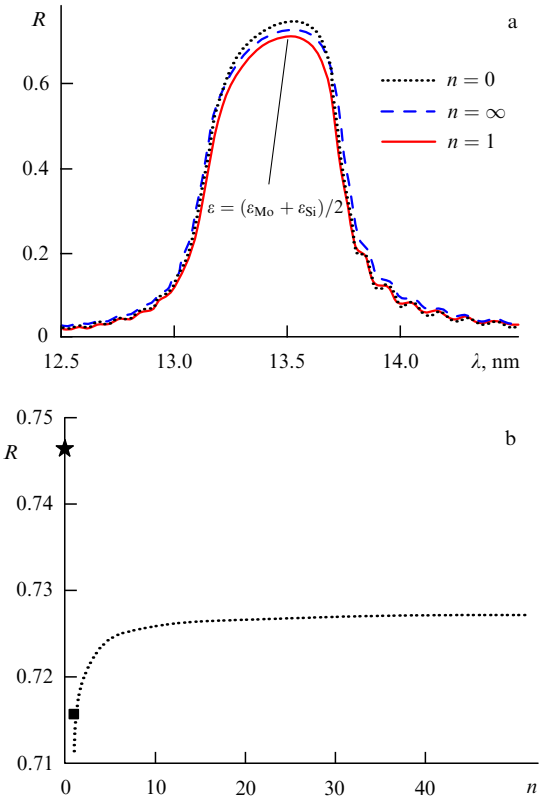

Figure 3. (a) Calculated spectral profile of the reflection coefficient of an Mo/Si periodic multilayer structure (150 layers) optimized for maximum reflection coefficient at $\lambda_0 = 13.5$ nm without the inclusion of transition layers (dotted curve, $n = 0$), with the inclusion of one transition layer with $\varepsilon = (\varepsilon_{Mo} + \varepsilon_{Si})/2$ (solid curve, $n = 1$) or a smooth transition of ε from ε_{Mo} to ε_{Si}, i.e., for $n \to \infty$ (dashed curve). (b) Calculated peak reflectivity without the inclusion of transition layers (star), with the inclusion of transition layers in the form of silicide $MoSi_2$ of thicknesses 6 Å (Si-on-Mo) and 12 Å (Mo-on-Si) (black square), as well as approximation of the smooth transition of ε by a different number of intermediate steps n.

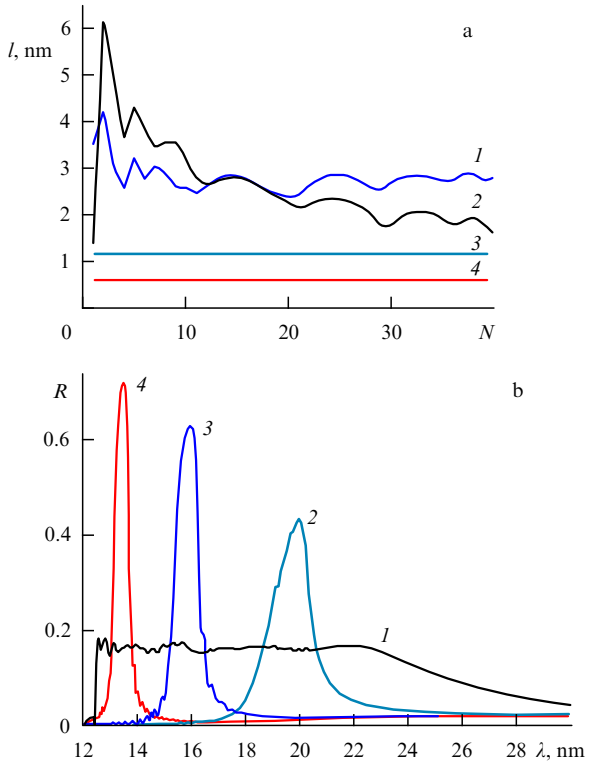

Figure 4. (Color online.) (a) Layer thicknesses l of Mo (1), Si (2), and transition (Mo-on-Si) (3) and (Si-on-Mo) (4) layers of aperiodic MS optimized for maximum uniform reflectivity in the 12.5–25 nm interval (the thicknesses of transition layers are fixed, the layer numbering increases downward from top to the substrate). (b) Calculated reflection coefficient of this aperiodic MS in the 12–30 nm range at normal radiation incidence (curve *1*). Shown for comparison are the reflection coefficients of periodic MMs optimized for maximum reflection coefficients at wavelengths of 20 nm (curve *2*), 16 nm (curve *3*), and 13.5 nm (curve *4*).

empirical rule whereby imposing the lower bound for a layer thickness at a level of $\approx \lambda_{min}/4$ (λ_{min} is the short-wavelength bound of the optimization interval) does not entail an appreciable lowering of the attainable (uniform) reflection coefficient.

3. Aperiodic normal-incidence Mo/Si multilayer mirrors and their application in experiments

Calculated at the first stage was an aperiodic MS (40-layer pairs of Mo and Si). The thicknesses $\{l_i\}$ of all 80 layers of Mo and Si were treated as independent variables (optimization parameters). The existence of $MoSi_2$ transition layers, which were formed in the structure synthesis, was also taken into account. Their thicknesses were assumed to be fixed and equal to 12 Å (Mo-on-Si) and 6 Å (Si-on-Mo). A structure of this type ($Si/MoSi_2/Mo/MoSi_2/\ldots Si/MoSi_2/Mo/MoSi_2/Substrate$) was optimized to achieve the highest possible uniform reflectivity throughout the 12.5–25 nm interval at normal radiation incidence.

Figure 4 shows the result of optimization: the layer thicknesses of the optimal aperiodic MS (Fig. 4a) and its calculated reflection coefficient in the 12.5–30 nm range (Fig. 4b). The integral reflectivity of this structure amounts to 1.97 nm in the interval $\lambda = 12.5-25$ nm and to 2.32 nm in the $\lambda = 12.5-30$ nm interval. In this case, the reflection coefficient averaged over the optimization interval $\lambda = 12.5-25$ nm is equal to 15.8%. Without the inclusion of transition layers, the average reflection coefficient of the corresponding optimized AMS is equal to 17.2%, i.e., the relative lowering of the 'plateau' level is equal to 8%.

The MSs corresponding to the calculated data were next deposited on concave spherical substrates by magnetron sputtering at KhPI. The synthesized MMs and witness mirrors were investigated at KhPI from the reflection of 1.54 Å radiation at grazing incidence; at the Institute for the Physics of Microstructures (IPM) of the Russian Academy of Sciences (RAS), their reflectivity was measured at several wavelengths in the operating range (12.5–30 nm) at normal incidence; at the Lebedev Physical Institute (LPI), RAS, the uniformity of reflection was estimated using a broadband laser-plasma source of VUV and SXR radiation. The synthesized MS proved to be sufficiently close to the calculated one and the relative uniformity of the reflection coefficient was $\approx 15\%$ [22, 24–26]. It is noteworthy that the reflection coefficient in the long-wavelength part of the operating range (25–30 nm) turned out to be somewhat higher than the calculated one.

The specified aperiodic MSs deposited on concave fused silica substrates 1.0 or 0.5 m in radius with a surface roughness of 3–5 Å were repeatedly employed to record spatially resolved plasma spectra with the use of the spectro-

graph represented schematically in Fig. 1a. Below, we describe several examples that demonstrate the virtues of this imaging (stigmatic) spectrograph.

We estimated the spatial, spectral, and temporal characteristics of a debris-free SXR radiation source excited in a pulsed xenon jet in a vacuum [27–29]. In the experiment, we recorded the resultant plasma spectrum in the 12.5–25 nm range, quasimonochromatic plasma images formed by radiation with the wavelengths $\lambda \approx 13.5$ and 18 nm, the absolute intensity of emission at these wavelengths, and the temporal shape of quasimonochromatic SXR radiation pulses.

Figure 5 shows an image of xenon plasma formed by its 13.5 nm radiation, which was recorded using a periodic MM with the reflectivity peak at $\lambda \approx 13.5$ nm in combination with a free-standing multilayer Zr/Si absorption filter.

In the xenon spectrum, we observed about one hundred spectral lines and unresolved line groups in the 12.5–25 nm range. Figure 6 shows one Xe spectrogram indicating several identified lines belonging to the ions Xe VIII–Xe X. The maximum of the Xe emission spectrum falls in the 14.5–17 nm range. The decrease in emission intensity for $\lambda < 14.5$ nm is due to photoabsorption in the relatively cool periphery of the xenon jet that surrounds the plasma volume radiating in the SXR region. This is borne out, in particular, by the fact that the short-wavelength intensity decrease in the spectrum changes upon varying the laser beam axis position relative to the jet axis; in this case, the thickness of the absorbing layer along the line of sight is varied. This absorption may be so strong that the radiation with wavelengths shorter than ≈ 15 nm emanating from the central part of the plasma column is almost completely absorbed, only the emission from the upper and lower parts of the column being observable. The observed 'splitting' begins in the $\lambda \approx 16-17$ nm range and increases with decreasing the wavelength to become as large as 1.3 mm, the jet diameter at the base at a distance of 0.5 mm from the nozzle. Shown at the bottom of Fig. 6 is the calculated transmittance of a 0.5 mm thick layer of neutral xenon with the atomic number density 2.2×10^{18} cm^{-3}. We can see that the absorption becomes stronger with a decrease in wavelength from 20 to 12.5 nm, where the optical thickness is $\tau = \mu_a n_{\mathrm{Xe\,I}} r \approx 3$ (μ_a is the photoabsorption cross section, $n_{\mathrm{Xe\,I}}$ is the number density of XeI, and r is the jet radius). The strong photoabsorption in the range of interest is primarily due to photodetachment of a 4d-electron in neutral Xe I. (The 4d-electron binding energy in neutral xenon is equal to 69.5 eV, which corresponds to a wavelength of 17.8 nm.)

Thus, the stigmatism of the spectrometer enabled demonstrating the role of reabsorption in the formation of the spatio-spectral picture of the emission intensity of the laser-plasma SXR source excited in an Xe jet in a vacuum.

We carried out the spectroscopic investigation of the charge exchange of multiply charged ions of laser plasma with the atoms of a rare-gas jet in a vacuum [30, 31]. The laser plasma was produced by irradiating solid targets with the output pulses of a neodymium-doped yttrium orthoaluminate crystal laser (Nd:$YAlO_3$, 0.5 J, 6 ns, 1.08 μm). The axis of the gas jet was parallel to the target plane and passed at a distance of ~ 1 cm from it (Fig. 7). The multiply charged ion flux produced by focusing the nanosecond laser pulses on the solid target was directed onto a supersonic jet to give rise to

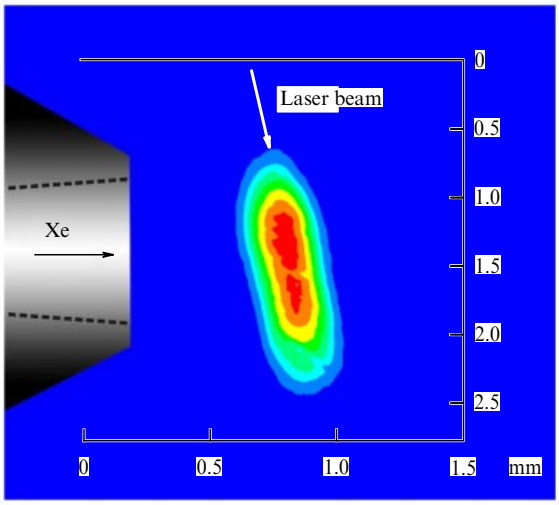

Figure 5. (Color online.) Quasi-monochromatic image of the xenon plasma produced by radiation with a wavelength of 13.5 nm, which was recorded using a periodic MM with a reflectivity peak at $\lambda \approx 13.5$ nm in combination with a free-standing multilayer Zr/Si absorption filter rejecting visible and UV radiation. Shown schematically at the left of the drawing is the nozzle of the gas valve.

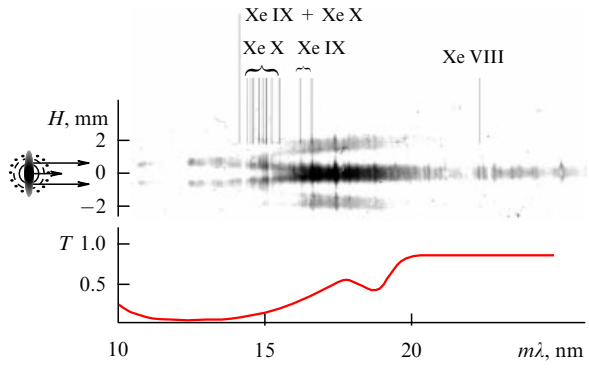

Figure 6. (Color online.) Spectrogram of Xe emission indicating several identified lines belonging to the ions Xe VIII – Xe X and the transmittance T of a 0.5-mm-thick Xe layer with the atomic number density 2.2×10^{18} cm^{-3}. H is the vertical coordinate in the xenon plasma, along which it was possible to obtain spatial resolution in the spectrum presented in the figure.

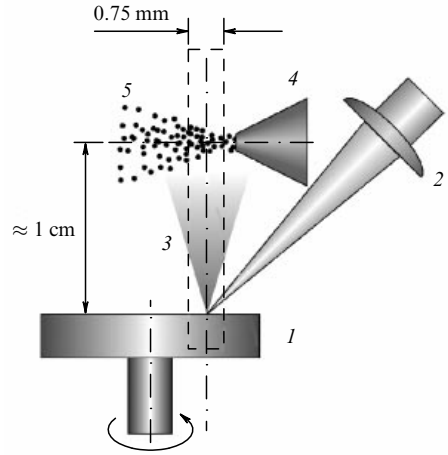

Figure 7. Mutual arrangement of a laser-plasma expansion cone and a rare-gas jet: *1* — rotatable target, *2* — lens, which focuses laser radiation, *3* — laser-produced plasma, *4* — nozzle of a pulsed gas valve, *5* — gas jet (the dashed lines show the field of view of the spectrograph).

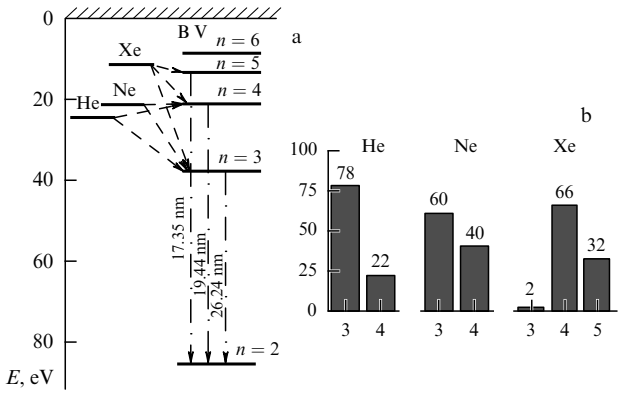

Figure 8. (a) Diagram of the charge exchange of boron nuclei (B VI) with He, Ne, and Xe rare-gas atoms. The dashed arrows show the electron transitions from a donor atom to a B V multiply charged ion, the dashed-dotted lines indicate the observable transitions of the Balmer series. (b) Variation of the distribution of the partial charge-exchange cross sections over the levels of B V ions with a change of the gas.

charge exchange in the interaction region. The field of view of the spectrograph (marked with dashed lines in Fig. 7) amounted to 20 mm vertically and covered both the region of laser-plasma emission and the charge-exchange region, making it possible to record the spatial picture of the plasma–gas interaction. The axis of the plasma plume cone was spaced 15 mm from the entrance slit, such that the radiation detection field, in view of the spectrograph acceptance angle, measured 0.75 mm in width. The simultaneous recording of a large number of spectral lines arising from the charge-exchange region enabled acquiring information about the distribution of charge-exchange products over the ion charge states and energy levels.

In the irradiation of a boron target, we recorded the charge exchange of B^{5+} nuclei with He, Ne, and Xe atoms (with ground-state ionization potentials of 24.6, 21.6, and 12.1 eV), which was attended by the population of the excited states of hydrogen-like B V ions with $n = 3$, 4, and 5 (Fig. 8a). The experiment involved recording the spectral lines arising from the Balmer series transitions H_α ($3 \to 2$, $\lambda = 26.24$ nm), H_β ($4 \to 2$, $\lambda = 19.44$ nm), and H_γ ($5 \to 2$, $\lambda = 17.35$ nm). The partial charge-exchange cross sections were estimated from the relative intensities of the Balmer lines (with the inclusion of cascade radiative transitions) (Fig. 8b). As the ionization potential of the donor atoms lowered, the 'center of gravity' of charge exchange shifted toward higher n, which reflected the quasiresonance nature of the charge exchange [40].

In Ref. [31], the interaction of multiply charged F and Li ions with Ne atoms in a pulsed gas jet was investigated. A rotating LiF disc was used as a target; the spectral lines of Li ions facilitated spectrum identification (Fig. 9). The charge exchange of the multiply charged ions of fluorine and lithium was recorded from the line spectra in the 125–350 Å range arising from the radiative decay of excited states of LiII–LiIII and FIII–FVIII ions populated in the course of the charge exchange. From the plasma–gas interaction region, it was possible to record transitions arising from the states of FIII–FVI ions with an open (partly or completely unfilled) 2s shell, which was indicative of the contribution of two- and multi-electron charge exchange of F ions with Ne atoms. For instance, the radiative transition $2p4s \to 2p^2$ (129.5 Å line) in the FVI ion testifies to the two-electron

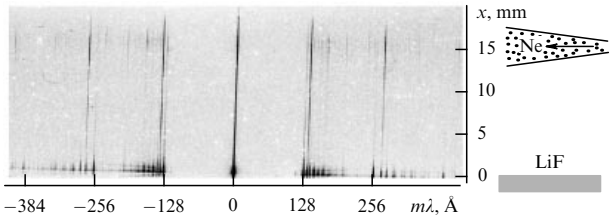

Figure 9. Spatio-spectral picture of the charge exchange of lithium and fluorine ions with neon jet atoms; x is the distance (in the plasma) from the LiF target surface. Spatial resolution in the spectrum presented in the figure was obtained along this direction.

charge exchange of the FVIII acceptor ion, the transition $2s2p(^3P^0)4d(^4D^0) \to 2s2p^2(^4P)$ (132.5 Å line, FV ion) to the two-electron charge exchange of the FVII acceptor ion, and the transition $2p^2(^3P)3p(^4D^0) \to 2s2p^2(^4P)$ (136.9 Å line) to the three-electron charge exchange of the FVIII acceptor ion.

In an experiment performed at the Advanced Photon Research Center, Japan Atomic Energy Agency, broadband Mo/Si MM optimized for maximum uniform reflectivity in the 12.5–25 nm range at an incidence angle of 5° was employed to record the SXR spectra of radiation reflected from a relativistic 'flying mirror' [33–35]. In this experiment, a slitless SXR spectrograph was used, which was aligned according to the setup in Fig. 2a. The role of detector was played by a backside-illuminated CCD.

Figure 10 shows the spectrum produced when the pulse of a femtosecond Ti:sapphire laser is reflected from the relativistic breaking plasma wake wave (the flying mirror) driven by another femtosecond pulse of the multiterawatt laser. The visible-to-SXR radiation conversion took place due to the double Doppler effect. The stigmatism of the spectrograph also permitted obtaining an upper estimate of the size of the SXR radiation source and investigating the relation between the source position and the delay between laser pulses.

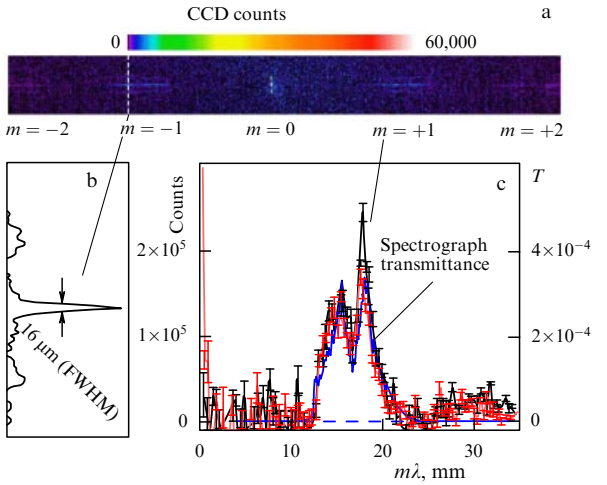

Figure 10. (Color online.) (a) Spectrum of the radiation reflected from a relativistic 'flying mirror' [33–35]; part of the image recorded with an X-ray CCD detector; we can see several orders of diffraction by the grating (5000 lines per mm) and its support structure (250 lines per mm, perpendicular to the main grating lines); (b). Vertical lineout of the spectrum in the −1st diffraction order, which characterizes the size (FWHM) of the SXR radiation source. (c) Emission spectra in the 1st and −1st diffraction orders, and the spectrograph transmittance vs the wavelength.

4. Broadband normal-incidence multilayer mirrors in the wavelength range $\lambda \leqslant 12.5$ nm

Advancement beyond the L edge of silicon, i.e., to the wavelength region below 12.5 nm, invites the use of material pairs other than Mo/Si. An analysis of the optical constants of elements suggested that the best results would be expected from uranium-bearing multilayer structures (naturally, the case in point is depleted uranium, which is composed primarily of ^{238}U). We carried out calculations of different aperiodic MSs in the range 6.7–11.1 nm, which rely on the optical constants of pure materials [41, 42]. Specifically, the calculations show that an aperiodic U/B_4C multilayer structure is capable of affording a uniform reflectivity of $\sim 7.5\%$ throughout the 6.7–11.1 nm wavelength interval and a U/C structure can provide a reflectivity of $\sim 4\%$ throughout the 4.4–7 nm interval. Quite good results can be expected from La/B_4C ($\sim 4.2\%$) in the 6.7–11.1 nm region (Fig. 11).

Several papers are concerned with the optical properties of uranium-containing mirrors [43–45]. At the same time, to our knowledge there are no reports in the literature about the synthesis of stable MMs with nanolayers of chemically pure uranium. This is hindered by the high chemical activity of uranium (it oxidizes and becomes friable, unless the uranium film is under ultrahigh vacuum conditions). In their analysis of the problem of fabrication of stable MMs based on uranium-bearing materials, the authors of Ref. [46] arrived at the conclusion that for the $\lambda > 4.5$ nm range, it is expedient to use uranium carbides (UC, U_2C_3) and possibly a three-component $(UC)_{1-x}(UN)_x$ substance. However, it is evident that the advantage of uranium as the bearer of favorable optical constants must wane as the fraction of uranium atoms in the uranium-containing layer decreases.

The synthesis of La/$B_4C(B_9C)$ MMs for a wavelength of ≈ 6.7 nm has been reported several times [47, 48]; however, the normal-incidence reflection coefficients of these mirrors turned out to be significantly lower than the theoretical limit, which was attributable to the formation of relatively thick transition layers. Recent progress in making La/B_4C multilayer structures achieved by the team of Salashchenko et al. [49] gives hope for the synthesis of aperiodic MMs based on these MSs for spectroscopy in the 6.6–11.0 nm range. In Ref. [49], it was possible to largely suppress the formation of transition layers in the La/B_4C structure due to the use of extremely thin (≈ 0.3 nm) carbon barrier layers and thereby attain a record value of reflectivity (58.6%) for a periodic structure at $\lambda = 66.6$ nm for a near-normal radiation incidence. This supposedly makes the La/B_4C structure the best candidate for the future synthesis of broadband aperiodic MMs for the 6.6–11.0 nm wavelength domain.

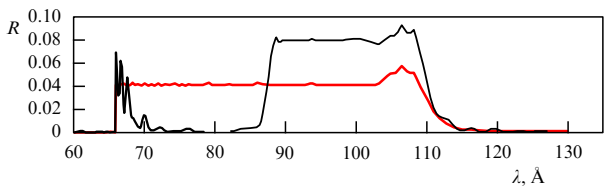

Figure 11. (Color online.) Calculated normal-incidence reflection coefficient R of aperiodic La/B_4C mirrors (200 layers) optimized for maximum uniform reflectivity in the wavelength intervals 66–110 and 88–110 Å.

5. Broadband polarization elements based on aperiodic structures

In Ref. [11], it was also pointed out that aperiodic MSs may fulfill the function of broadband polarizer mirrors for a fixed angle of radiation incidence. It was found that aperiodic MSs optimized for uniform reflectivity at an incidence angle close to Brewster's angle have a very high (but not 100%) polarizance throughout the spectral interval of optimization and may serve as efficient radiation polarizers. Simulations were made of aperiodic MSs optimized for uniform reflectivity over the wavelength ranges 8.8–12.4 nm (an Rh/B_4C structure, optimal incidence angle $\theta = 42.5°$), $\lambda = 13-19$ nm (Mo/Si, $\theta = 41°$), and $\lambda = 19-30$ nm ($MoSi_2$/Si, $\theta = 41.5°$), which were virtually nonreflective to p-polarized radiation in the corresponding spectral subdomains. Specifically, the polarizance $P(\lambda) = (R_s - R_p)/(R_s + R_p)$ of the Mo/Si polarizer varied from 1.00 to 0.94 in the operating range (13–19 nm) to decrease to 0.88 for $\lambda = 20$ nm (Fig. 12). In this case, the calculated reflection coefficient for s-polarized radiation amounted to 34% (without the inclusion of transition layers). The merit of optical components of this kind is that tuning the radiation wavelength is not attended by rotation of the polarizer, and the ray paths in an optical system remain invariable.

Interest in such polarizers has been shown by foreign research centers, presumably due to the pursuance of polarization measurements with the use of synchrotron radiation. In the USA, a similar single-mirror polarizer centered at a wavelength of about 14.25 nm with a spectral width of approximately 3 nm was synthesized in Ref. [50]; in doing this, when calculating this structure, the authors took into account the formation of transition layers in the form of silicide $MoSi_2$ of a fixed thickness (see Section 2.2). Due to this circumstance, the measured reflection coefficient for s-polarized radiation (≈ 0.2) agreed nicely with the calculated one and was reasonably uniform (Fig. 13).

At the Institute of Precision Optical Engineering (Tongji University, Shanghai, China), systematic research is carried out to develop broadband X-ray optical elements based on aperiodic MSs with the use of different material pairs. The authors of Ref. [51] reported the synthesis of three broad-

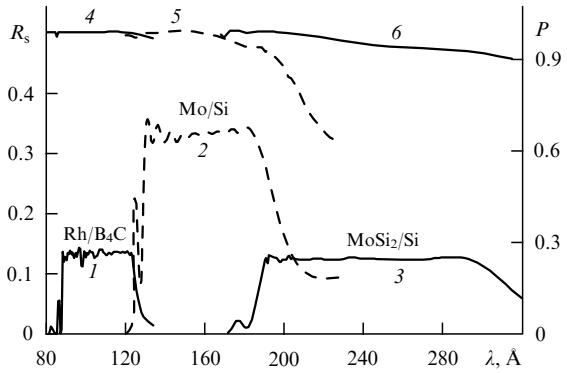

Figure 12. Reflection coefficients (*1–3*) for s-polarized radiation and polarizances (*4–6*) of three aperiodic MMs optimized for maximum uniform reflectivity in the wavelength ranges 88–124 Å (Rh/B_4C, $\theta \approx 42.5°$, $N = 120$) (curves *1*, *4*), 130–190 Å (Mo/Si, $\theta \approx 41°$, $N = 40$) (curves *2*, *5*), and 190–300 Å ($MoSi_2$/Si, $\theta \approx 41.5°$, $N = 20$) (curves *3*, *6*).

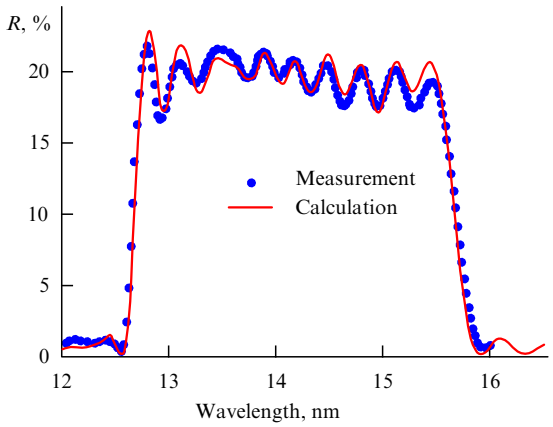

Figure 13. (Color online.) Calculated (solid curve) and measured (dots) reflection coefficients of an aperiodic MM polarizer ($\theta = 45°$) (borrowed from Ref. [50]). The model takes into account the existence of transition layers with a stoichiometry of $MoSi_2$.

band polarizers based on aperiodic Mo/Si structures for the wavelength ranges 15–17 nm, 14–18 nm, and 13–19 nm. In all three cases, the measured $P(\lambda)$ values turned out to be close to the calculated ones throughout the working wavelength intervals, the measured values averaged over the respective working intervals being equal to 0.987, 0.986, and 0.980. The reflection coefficients turned out to be somewhat lower than the calculated ones and varied within 36–38, 17–25, and 15–27%, while the respective calculated averages were equal to 50.0, 35.0, and 30.4.

Reported in Ref. [52] was the synthesis of broadband Mo/Y polarizers for the wavelength ranges 8.5–10.1 nm and 9.1–11.7 nm with reflectivities of 5.5% and 6.1% for s-polarized radiation. The respective average measured polarizance was equal to $(98.79 \pm 0.32)\%$ and $(96.48 \pm 0.70)\%$.

A phase-shifting transmission optical element was calculated and synthesized in Ref. [53], which was an aperiodic multilayer Mo/Si structure deposited on a silicon nitride membrane. The measured phase shift between s- and p-polarized radiation was equal to 42° in the 13.8–15.5 nm wavelength range for an angle of oblique incidence of 47°.

A brief review of the investigations of all kinds of aperiodic MSs carried out at the Institute of Precision Optical Engineering is given in Ref. [54].

Research on quarter-wave plates for SXR radiation, which are intended for operation in transmitted [55] or reflected [56] beams, is conducted at the Beijing University of Chemical Technology jointly with the China University of Geosciences (Beijing). It was noted that moving to aperiodic structures permits a significant improvement in the characteristics of quarter-wave plates. An aperiodic Mo/Si structure was calculated for fulfilling the function of a transmission quarter-wave plate at an incidence angle of about 45° for radiation with an energy of 90 eV [55]. Also, an aperiodic Mo/Si MM was calculated, which can serve as a broadband quarter-wave plate in the ≈ 80–100 eV range at a grazing-incidence angle of 30° [56]. The authors of Ref. [56] believe that the development of broadband quarter-wave plates will make it possible to control the state of polarization of ultrashort SXR radiation pulses, in particular, of the high-order harmonics of femtosecond lasers.

6. Aperiodic multilayer mirrors as elements of attosecond soft X-ray optics

As pointed out in Refs [12, 13], aperiodic MMs are capable of reflecting attosecond pulses of SXR radiation (consisting of only a few wave cycles) at normal incidence and hard X-ray pulses at oblique incidence with retention of their temporal shape, as well as of compressing chirped pulses in time, similarly to the mirrors for femtosecond pulses of the visible and infrared spectral ranges [57]. Of special interest are normal-incidence MMs, which may be realized in the SXR region at an acceptable level of reflectivity. The minimal pulse duration expressed in terms of wave periods is equal to the relative width of the pulse spectrum, $\delta\omega_p/\omega_0 \sim T/\tau$ (here, ω_0 is the carrier frequency, $\delta\omega_p$ is the spectrum width, T is the wave period, and τ is the pulse duration). In particular, when a pulse contains only several oscillation cycles (a few-cycle pulse), the width of its spectrum is comparable to the carrier frequency. Periodic MMs exhibit a resonance frequency dependence of their reflection coefficients ($\Delta\omega/\omega_0 \sim 0.05-0.01$) and are therefore capable of retaining the pulse shape only for pulses that contain no fewer than several dozen wave periods. To reflect extremely short X-ray pulses, aperiodic MMs with a broad reflection spectrum must be used.

Let $r(\omega) = |r(\omega)| \exp\left[i\Phi(\omega)\right]$ be the complex amplitude reflection coefficient of some (not necessarily periodic) MS and $\Phi(\omega)$ be its phase. Then the delay of the reflected pulse relative to the incident one is equal to the group delay

$$t_g = \left.\frac{d\Phi(\omega)}{d\omega}\right|_{\omega=\omega_0},$$

and its spreading in time is determined by the group delay dispersion and its spectral width $\sim (dt_g/d\omega)\,\delta\omega_p$. A sufficient condition for the retention of the pulse shape at reflection is a uniform reflection coefficient in a broad spectral region in combination with a zero group delay dispersion ($d^2\Phi(\omega)/d\omega^2 = 0$) throughout the spectral region. Simulations in [12, 13] suggest that in the 65–95 eV energy range, this requirement can be fulfilled for an energy reflection coefficient of 7%, the aperiodic Mo/Si MM retaining the shape of SXR pulses for a pulse duration down to 0.15 fs [12, 13]. In dealing with chirped pulses of the form

$$E_0(t) = \exp\left[-\frac{\pi}{2}\left(\frac{t}{\tau_0}\right)^2\right]\cos\left(\omega_0 t - bt^2\right), \quad b > 0,$$

it is possible to compress the incident pulse in its reflection from an aperiodic MM (E_0 is the amplitude of the electric field of the wave). In this case, a sufficient condition for the compression of a chirped pulse is a uniform reflection in combination with a group delay of the form $t_g = d\Phi(\omega)/d\omega \approx t_{g0} + 0.5b^{-1}(\omega - \omega_0)$. The aperiodic mirror optimized to satisfy this condition should perform a tenfold compression of a pulse with a duration (FWHM) of 1.5 fs (down to 0.15 fs) (Fig. 14). In this case, the power 'reflection coefficient' may be greater than unity due to the time compression, despite the energy loss.

We note that it is the power of ultrashort pulses that is of paramount importance in many experiments of different kinds. In such cases, it would be reasonable to select the goal function in the form of the peak power $P_0 = W_0/\tau_{eff}$, where W_0 is the pulse energy and $\tau_{eff} = \int P(t)\,dt$ is its effective

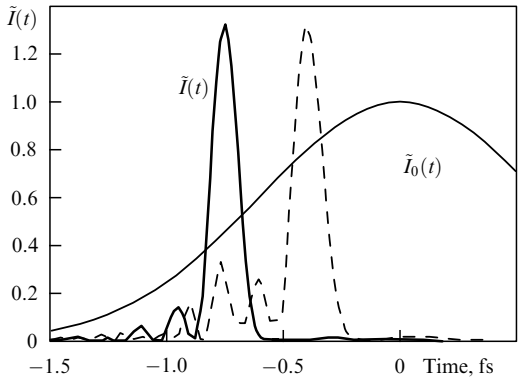

Figure 14. Temporal chirped-pulse compression to a duration of 0.15 fs (FWHM) with the use of an aperiodic MS.

duration; the area under the $P(t)$ curve, where $P(t)$ is the normalized instantaneous pulse power, is therefore such that $\max[P(t)] = 1$. In this instance, no additional conditions are imposed on the profile of the reflection coefficient and its phase. This approach was used in [58] to calculate a mirror that performed more than a twofold increase in power for a negatively chirped pulse 2.5 fs in duration; in this case, its effective duration decreased 13-fold for an energy reflection coefficient of 0.17.

Finally, when incident pulses are positively chirped ($b < 0$), as may be the case in the generation of high-order harmonics of femtosecond laser pulses, it is also possible to design a multilayer mirror (Mo/Si) with a negative group delay dispersion, which compensates this chirp and compresses the pulses to a duration of ≈ 100 as [58, 59]. In this case, the goal function was specified in Ref. [58] for the power of the reflected pulse, while in Ref. [59] a combination of the spectral reflectivity profile and the phase was used, as described in the foregoing (an example is provided in Fig. 14).

At present, work to develop MMs capable of manipulating SXR radiation pulses of the order of 100 as in duration has passed from the stage of purely theoretical investigation to the stage of practical realization: there is a growing body of literature on these developments (see, e.g., Refs [60–66]).

7. Conclusions

To date, the optics of the SXR spectral range have seen the formation of the research area of aperiodic multilayer optics. The application of aperiodic structures broadens the capabilities of multilayer optics and makes it possible to satisfy several optimization criteria other than attainment of the highest possible reflection coefficient in a relatively narrow range of wavelengths (or angles of incidence). Mo/Si multilayer structures having uniform reflectivity in a broad spectral range (12.5–25 nm) at normal radiation incidence have been synthesized and employed in spectroscopy. The possibility of using broadband aperiodic MMs (Mo/Si, Al/Zr, Al/Sc) in space-based instruments intended for spectroscopic observations of the solar corona in the 17–21, 24–28, and 28–33 nm wavelength ranges is being studied theoretically and experimentally [67].

In foreign laboratories, keen interest is shown in the synthesis of broadband polarizers operating at constant incidence angles, as well as of quarter-wave plates operating in transmission or reflection modes. Advancement to the $\lambda < 12.5$ nm domain is possible with the use of other material pairs than Mo/Si and may be achieved at the expense of some lowering of uniform reflection coefficients. Simulations suggest that it is possible to obtain $\bar{R} \approx 10\%$ throughout the 9 – 13 nm range and about 4% throughout the 6.6–11 nm range. Research is underway to make aperiodic MMs for application in attosecond optics. In the range $\lambda \sim 100-200$ Å, this will allow manipulating ultrashort few-cycle SXR pulses down to ~ 100 as in duration.

Acknowledgements
This research was supported by the Russian Science Foundation (project No. 14-12-00506).

References

1. Spiller E *Appl. Phys. Lett.* **20** 365 (1972)
2. Vinogradov A V, Zeldovich B Ya *Opt. Spectrosc.* **42** 404 (1977); *Opt. Spektrosk.* **42** 709 (1977)
3. Vinogradov A V, Kozhevnikov I V *Tr. Fiz. Inst. Akad. Nauk SSSR* **196** 62 (1989)
4. Spiller E A *Proc. SPIE* **1546** 489 (1992)
5. Barysheva M M et al. *Phys. Usp.* **55** 681 (2012); *Usp. Fiz. Nauk* **182** 727 (2012)
6. Corkum P B *Phys. Rev. Lett.* **71** 1994 (1993)
7. Teubner U, Gibbon P *Rev. Mod. Phys.* **81** 445 (2009)
8. Cingöz A et al. *Nature* **482** 68 (2012)
9. Jones R J et al. *Phys. Rev. Lett.* **94** 193201 (2005)
10. Samson J A R *Techniques of Vacuum Ultraviolet Spectroscopy* (New York: Wiley, 1967)
11. Kolachevskii N N, Pirozhkov A S, Ragozin E N *Quantum Electron.* **30** 428 (2000); *Kvantovaya Elektron.* **30** 428 (2000)
12. Beigman I L, Pirozhkov A S, Ragozin E N *JETP Lett.* **74** 149 (2001); *Pis'ma Zh. Eksp. Teor. Fiz.* **74** 167 (2001)
13. Beigman I L, Pirozhkov A S, Ragozin E N *J. Opt. A Pure Appl. Opt.* **4** 433 (2002)
14. Meekins J F, Cruddace R G, Gursky H *Appl. Opt.* **26** (6) 990 (1987)
15. van Loevezijn P et al. *Appl. Opt.* **35** 3614 (1996)
16. Balakireva L L, Kozhevnikov I V *J. X-Ray Sci. Technol.* **6** 150 (1996)
17. Joensen K D et al. *Proc. SPIE* **2279** 180 (1994)
18. Kozhevnikov I V, Bukreeva I N, Ziegler E *Nucl. Instrum. Meth. Phys. Res. A* **460** 424 (2001)
19. Ziegler E et al. *Proc. SPIE* **3737** 386 (1999)
20. Morawe Ch et al. *Nucl. Instrum. Meth. Phys. Res. A* **493** 189 (2002)
21. Kozhevnikov I V, Montcalm C *Nucl. Instrum. Meth. Phys. Res. A* **624** 192 (2010)
22. Kondratenko V V et al. *Kratk. Soobshch. Fiz. Fiz. Inst. Ross. Akad. Nauk* (7) 32 (2001)
23. Vishnyakov E A, Shatokhin A N, Ragozin E N *Quantum Electron.* **45** 371 (2015); *Kvantovaya Elektron.* **45** 371 (2015)
24. Ragozin E N et al. *Proc. SPIE* **4782** 176 (2002)
25. Vishnyakov E A et al. *Quantum Electron.* **39** 474 (2009); *Kvantovaya Elektron.* **39** 474 (2009)
26. Ragozin E N et al. *Proc. SPIE* **7360** 73600N (2009)
27. Kapralov V G et al. *Quantum Electron.* **32** 149 (2002); *Kvantovaya Elektron.* **32** 149 (2002)
28. Levashov V E et al. *Radiat. Phys. Chem.* **75** 1819 (2006)
29. Levashov V E et al. *Quantum Electron.* **36** 549 (2006); *Kvantovaya Elektron.* **36** 549 (2006)
30. Beigman I L et al. *Quantum Electron.* **37** 1060 (2007); *Kvantovaya Elektron.* **37** 1060 (2007)
31. Beigman I L et al. *Quantum Electron.* **40** 545 (2010); *Kvantovaya Elektron.* **40** 545 (2010)
32. Louis E et al. *Proc. SPIE* **7361** 73610I (2009)
33. Kando M et al. *Phys. Rev. Lett.* **103** 235003 (2009)
34. Pirozhkov A S et al. *AIP Conf. Proc.* **1153** 274 (2009)
35. Pirozhkov A S et al. *Proc. SPIE* **8140** 81400A (2011)
36. Henke B L, Gullikson E M, Davis J C *Atom. Data Nucl. Data Tabl.* **54** 181 (1993)
37. Soufli R, Gullikson E M *Proc. SPIE* **3113** 222 (1997)

38. Parratt L G *Phys. Rev.* **95** 359 (1954)
39. Zubarev E N et al. *Metallofiz. Noveish. Tekhnol.* **19** (8) 56 (1997)
40. Janev R K, Presnyakov L P, Shevelko V P *Physics of Highly Charged Ions* (Springer Series in Electrophysics, Vol. 13) (Berlin: Springer-Verlag, 1985) p. 151
41. Zhivlyuk G M et al., in *Nanofizika i Nanoelektronika*: *XI Mezhdunar. Simpozium, Nizhnii Novgorod, 10–14 Marta 2007 g.* (Nanophysics and Nanoelectronics: XIth Intern. Symp., Nizhny Novgorod, 10–14 March 2007) Vol. 2 (Nizhny Novgorod: Institute for Physics of Microstructures RAS, 2007) p. 361
42. Vishnyakov E A et al. *Quantum Electron.* **42** 143 (2012); *Kvantovaya Elektron.* **42** 143 (2012)
43. Allred D D et al. *Proc. SPIE* **4782** 212 (2002)
44. Sandberg R L et al. *Proc. SPIE* **5193** 191 (2004)
45. Artyukov I A et al. *Poverkhnost Rentgen. Sinkhrotron. Neitron. Issled.* (5) 9 (2007)
46. Artioukov I A et al. *Nucl. Instrum. Meth. Phys. Res. A* **517** 372 (2004)
47. Platonov Yu Yu, Gomez L, Broadway D *Proc. SPIE* **4782** 152 (2002)
48. Barysheva M M et al., in *Rentgenovskaya Optika – 2008. Materialy Soveshchaniya, g. Chernogolovka, 6–9 Oktyabrya 2008 g.* (X-Ray Optics – 2008. Conf. Proc., Chernogolovka, 6–9 October 2008) (Chernogolovka: Inst. of Microelectronics Technology and High-Purity Materials RAS, 2008) p.32; http://purple.iptm.ru/xray/xray2008/files_files/X-ray%202008.pdf
49. Chkhalo N I et al. *Appl. Phys. Lett.* **102** 011602 (2013)
50. Aquila A L et al. *Opt. Express* **14** 10073 (2006)
51. Wang Z et al. *J. Appl. Phys.* **99** 056108 (2006)
52. Wang Z et al. *Appl. Phys. Lett.* **89** 241120 (2006)
53. Wang Z et al. *Appl. Phys. Lett.* **90** 031901 (2007)
54. Wang Z et al. *Chinese Opt. Lett.* **8** 163 (2010)
55. Lin C, Chen S, Chen Z *Opt. Commun.* **326** 70 (2014)
56. Lin C, Chen S, Chen Z, Ding Y *Opt. Commun.* **347** 98 (2015)
57. Szipöcs R et al. *Opt. Lett.* **19** 201 (1994)
58. Pirozhkov A S et al., in *Ultrafast Phenomena XIV*: *Proc. 14th Intern. Conf., Niigata, Japan, July 25–30, 2004* (Eds T Kobayashi et al.) (Berlin: Springer, 2005) p. 85
59. Morlens A-S et al. *Opt. Lett.* **30** 1554 (2005)
60. Wonisch A et al. *Appl. Opt.* **45** 4147 (2006)
61. Aquila A, Salmassi F, Gullikson E *Opt. Lett.* **33** 455 (2008)
62. Hofstetter M et al. *New J. Phys.* **13** 063038 (2011)
63. Guggenmos A et al. *Proc. SPIE* **8502** 850204 (2012)
64. Bourassin-Bouchet C et al. *New J. Phys.* **14** 023040 (2012)
65. Guggenmos A et al. *Proc. SPIE* **9207** 92070L (2014)
66. Diveki Z et al. *J. Mod. Opt.* **61** 122 (2014)
67. Vishnyakov E A et al., in *Nanofizika i Nanoelektronika*: *Trudy XIX Mezhdunar. Simpoziuma, Nizhnii Novgorod, 10–14 Marta 2015 g.* (Nanophysics and Nanoelectronics: Proc. XIXth Intern. Symp., Nizhny Novgorod, 10–14 March 2015) Vol. 1 (Nizhny Novgorod: Izd. Nizhegorodskogo Univ. im. N.I. Lobachevskogo, 2015) p. 326; http://nanosymp.ru/UserFiles/Symp/2015_v1.pdf